IVYSPRING INTERNATIONAL PUBLISHER

Theranostics

2017; 7(11): 2924-2939. doi: 10.7150/thno.20094

Research Paper

Al^{18}F-Labeling Of Heat-Sensitive Biomolecules for Positron Emission Tomography Imaging

Frederik Cleeren[1], Joan Lecina[1], Muneer Ahamed[1], Geert Raes[2, 3], Nick Devoogdt[4], Vicky Caveliers[4], Paul McQuade[5], Daniel J Rubins[5], Wenping Li[5], Alfons Verbruggen[1], Catarina Xavier[4] and Guy Bormans[1]✉

1. Laboratory for Radiopharmaceutical research, Department of Pharmacy and Pharmacology, University of Leuven, Leuven, Belgium;
2. Laboratory of Cellular and Molecular Immunology, Vrije Universiteit Brussel, Brussels, Belgium;
3. VIB Laboratory of Myeloid Cell Immunology, Vrije Universiteit Brussel, Brussels, Belgium;
4. In Vivo Cellular and Molecular Imaging Center, Vrije Universiteit Brussel, Brussels, Belgium;
5. Translational Biomarkers, Merck Research Laboratories, Merck & Co., 770 Sumneytown Pike, West Point, Pennsylvania 19486, United States.

✉ Corresponding author.

Received: 2017.03.15; Accepted: 2017.06.02; Published: 2017.07.14

Abstract

Positron emission tomography (PET) using radiolabeled biomolecules is a translational molecular imaging technology that is increasingly used in support of drug development. Current methods for radiolabeling biomolecules with fluorine-18 are laborious and require multistep procedures with moderate labeling yields. The Al^{18}F-labeling strategy involves chelation in aqueous medium of aluminum mono[^{18}F]fluoride ({Al^{18}F}$^{2+}$) by a suitable chelator conjugated to a biomolecule. However, the need for elevated temperatures (100-120 °C) required for the chelation reaction limits its widespread use. Therefore, we designed a new restrained complexing agent (RESCA) for application of the AlF strategy at room temperature.

Methods. The new chelator RESCA was conjugated to three relevant biologicals and the constructs were labeled with {Al^{18}F}$^{2+}$ to evaluate the generic applicability of the one-step Al^{18}F-RESCA-method.

Results. We successfully labeled human serum albumin with excellent radiochemical yields in less than 30 minutes and confirmed *in vivo* stability of the Al^{18}F-labeled protein in rats. In addition, we efficiently labeled nanobodies targeting the Kupffer cell marker CRIg, and performed µPET studies in healthy and CRIg deficient mice to demonstrate that the proposed radiolabeling method does not affect the functional integrity of the protein. Finally, an affibody targeting HER2 (PEP04314) was labeled site-specifically, and the distribution profile of (±)-[^{18}F]AlF(RESCA)-PEP04314 in a rhesus monkey was compared with that of [^{18}F]AlF(NOTA)-PEP04314 using whole-body PET/CT.

Conclusion. This generic radiolabeling method has the potential to be a kit-based fluorine-18 labeling strategy, and could have a large impact on PET radiochemical space, potentially enabling the development of many new fluorine-18 labeled protein-based radiotracers.

Key words: Al^{18}F-labeling; PET; human serum albumin; nanobody; affibody.

Introduction

Positron emission tomography (PET) provides non-invasive, sensitive and specific imaging of molecular interactions *in vivo*, and can be used to study the function of cells, receptors, neurotransmitters, genes and drug pharmacokinetics [1]. Among positron-emitting radioisotopes, the halogen fluorine-18 is the most commonly used radionuclide due to its optimal chemical properties and favorable nuclear decay characteristics [2]. The low maximum positron energy (0.635 MeV) of fluorine-18 enables the acquisition of high resolution PET images as a result of the short range of tissue penetration prior to annihilation [3, 4]. Fluorine-18 has a half-life of 109.8 min, which is short enough to avoid prolonged irradiation of subjects, yet still long enough to allow extended *in vivo* investigations and

distribution to remote imaging centres without an on-site cyclotron [2, 5]. The success and medical impact of PET using 2-[^{18}F]fluoro-2-deoxy-D-glucose ([^{18}F]FDG), led to a fast worldwide proliferation of PET camera's and fluorine-18 producing cyclotron centres [6]. Consequently, fluorine-18 is now readily available in numerous hospitals and research centres, and the infrastructure is in place to expand its application far beyond [^{18}F]FDG [7].

In addition to using small organic molecules, researchers in the molecular imaging community are increasingly interested in using peptides and high molecular weight biomolecules for use as PET-radiopharmaceuticals, in line with the growth of the share of biologic- based drugs in the global pharmaceutical market [8]. The molecular imaging technique, immuno-PET, combines the high *in vivo* target affinity and selectivity of antibodies or antibody fragments and the high resolution and sensitivity of PET for imaging ligand-target interactions. An immuno-PET tracer should exhibit a high target-to-background ratio, high target specificity, high stability, sufficient solubility and low immunogenicity [9]. The advantage of using mAbs (150 kDa) as vector molecules in immuno-PET is their (sub)nanomolar affinity, excellent specificity and high accumulation at the target site [10]. Moreover, the availability of a large number of FDA-approved mAbs for imaging purposes can stimulate clinical translation [9]. However, as a result of the long residence time in blood of full-length antibodies, imaging with sufficient contrast between target and non-target tissues can only be performed several days post-injection, with peak contrast generally obtained after 2-4 days. Hence, due to the slow kinetics, radiolabeling with long-lived radionuclides such as zirconium-89 (^{89}Zr, $t_{1/2}$: 3.3 days) or iodine-124 (^{124}I, $t_{1/2}$: 4.2 days) is required, causing a high radiation burden for the patient (20-40 mSv per scan). The use of long-lived radionuclides is impractical for routine clinical use and, moreover, has a severe social impact on patients as only limited visiting time of family is advised for radioprotection reasons.

Advancements in biotechnology have led to the bioengineering of many vector molecules with shorter biological half-lives, and compatible with a short-lived PET radionuclide such as fluorine-18, that can be used as an alternative to mAbs [11]. Examples of suitable vector molecules are 80-kDa minibodies [12], 55-kDa antigen-binding fragments (Fab) [13], 28-kDa single-chain variable fragment (scFv) [14], 18-kDa designed ankyrin repeat proteins (DARPins) [15], 15-kDa antibody fragments derived from heavy-chain only antibodies (V_{HH} or nanobodies) [16], 7-kDa affibody molecules [17], 7-kDa albumin-binding domain derived affinity proteins (ADAPTs) [18] and many others [11]. These radiolabeled vector molecules are expected to play an increasingly important role in cancer diagnosis, treatment selection, and monitoring of molecularly targeted therapeutics. However, the incorporation of fluorine-18 into heat-sensitive and complex biomolecules creates substantial challenges for radiochemists, and so only a limited number of methods are currently available.

Conventional radiofluorination strategies involve carbon-fluorine bond formation in anhydrous aprotic solvents using aliphatic or aromatic nucleophilic substitution reactions, generally at high temperatures (**Figure 1A**). A solution to overcome the complications caused by the low nucleophilicity of [^{18}F]F$^-$ in aqueous media is the use of prosthetic groups (**Figure 1B**). Fluorine-18 labeled prosthetic groups (or secondary labeling agents) are small and simple fluorine-18 containing molecules that facilitate the radiolabeling process of complex molecules [19]. Some well-known prosthetic groups are *N*-succinimidyl 4-[^{18}F]fluorobenzoate ([^{18}F]SFB) [20], 6-[^{18}F]fluoronicotinic acid 2,3,5,6-tetrafluorophenyl ester ([^{18}F]F-Py-TFP) [21] and *N*-[2-(4-[^{18}F]fluoroben-zamido)ethyl]maleimide ([^{18}F]FBEM) [22]. This approach avoids exposing the biomolecule to harsh conditions, but intrinsically requires time-consuming synthetic procedures that often include several purification steps (e.g. HPLC). Hence, there is a need for innovative, efficient radiolabeling methods that will boost the use of fluorine-18 labeled biomolecules in PET research and clinical studies.

Several non-carbon elements favour strong bonds (*i.e.* high bond enthalpy) with fluorine, with preservation of high kinetic stability of the fluorine containing compounds formed. Moreover, lower activation energy is required for formation of these bonds in comparison to carbon-fluorine bonds [8]. This has been the basis for a new research field in ^{18}F-radiochemistry. Currently, boron, silicon and aluminum are being investigated as elements allowing fluorination in an aqueous environment. An excellent review by *Bernard-Gauthier et al.* deals with the current status of both the ^{18}F-SiFA and ^{18}F-BF_3 technologies for fluorine-18 labeling, and their use in preclinical PET imaging [23]. The strength of the inorganic approach is that it can entail a single, potentially very fast, radiochemical reaction step in, at least partially, aqueous media [8], that can be easily automated for routine production.

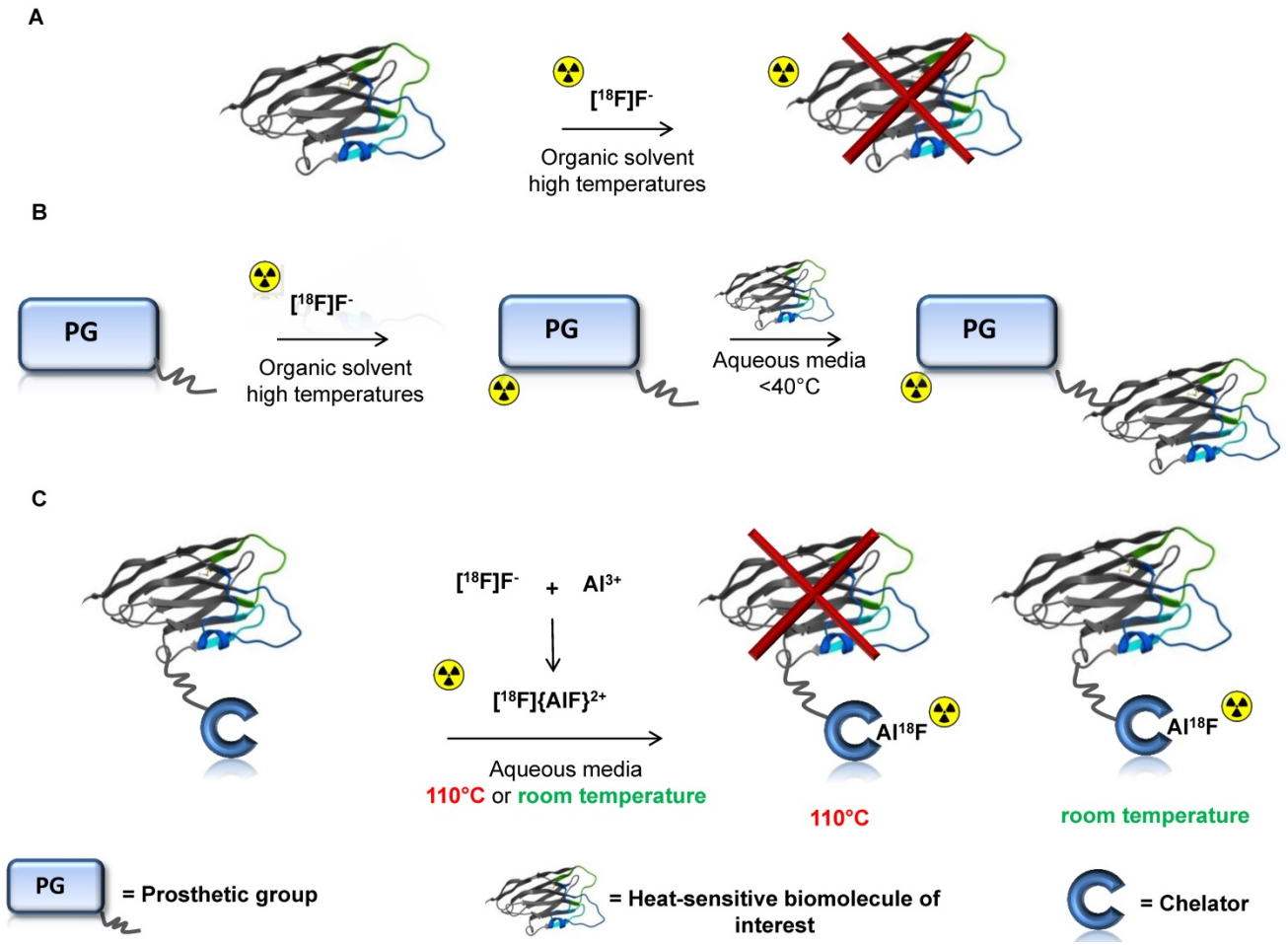

Figure 1. Overview of fluorine-18 radiolabeling methods for heat-sensitive biomolecules A: Conventional radiofluorination strategies in anhydrous aprotic solvents using aliphatic or aromatic nucleophilic substitution reactions at high temperatures are not compatible with heat-sensitive biomolecules **B:** Fluorine-18 labeled prosthetic groups facilitate the radiolabeling process of complex molecules. This approach avoids exposing the biomolecule to harsh conditions but intrinsically requires a time consuming synthetic procedure to obtain the radiolabeled prosthetic group that often includes several purification steps **C:** One-pot radiolabeling of biomolecules with fluorine-18 via the Al^{18}F-method at 110 °C using macrocyclic Al^{18}F-chelators (not compatible with heat-sensitive biomolecules) or at room temperature using a restrained complexing agent (RESCA) as Al^{18}F-chelator.

Al^{18}F-chelation is a relatively new strategy that allows one-pot radiofluorination of biomolecules in aqueous media [24]. In this method, fluorine is firmly bound to Al^{3+} (>670 KJ/mol), forming aluminum mono[^{18}F]fluoride ([^{18}F]{AlF}$^{2+}$), and this moiety is subsequently chelated by a suitable chelator conjugated to a biomolecule (**Figure 1C**) [25].

A wide range of peptides have been labeled using the Al^{18}F-method with macrocyclic chelators such as the pentadentate (N_3O_2-donor) ligand 1,4,7-triazacyclononane-1,4-diacetate (NODA) and the hexadentate (N_3O_3-donor) ligand 1,4,7-triazacyclononane-1,4,7-triacetate (NOTA) [26]. This has allowed radiolabeling with [^{18}F]{AlF}$^{2+}$ of relatively small peptides such as $\alpha_v\beta_3$ integrin-binding peptides [27], and also larger peptides, such as exendin-4 [28] and affibodies [29]. The first clinical study using peptides labeled *via* the Al^{18}F-method was published in 2013 [30]. Although the macrocyclic chelators used in these methods have shown a lot of potential, the approach has limited applicability due to the high temperature required for the complexation reaction (≥ 100 °C) [31]. These harsh reaction conditions are clearly not compatible with heat-sensitive biomolecules (**Figure 1C**).

Recently, we developed a new restrained complexing agent, ((±)-H_3RESCA), that allows efficient chelation of [^{18}F]{AlF}$^{2+}$ using mild labeling conditions. (±)-H_3RESCA is an acyclic pentadentate ligand with an N_2O_3 coordinative set of donor atoms. As a result, (±)-H_3RESCA showed excellent labeling properties at room temperature and its Al^{18}F-complex demonstrated high *in vitro* and *in vivo* stability. Indeed, the development of this new chelator makes it possible to radiolabel heat-sensitive biomolecules with fluorine-18 in one radiolabeling step (**Figure 1C**). The synthesis of this new chelator, in addition to the synthesis of bifunctional derivatives, in depth characterization of the corresponding Al^{18}F-complex, and evaluation of *in vitro* and *in vivo* stability of the

$Al^{18}F$-complex, is described in a patent [32] and will be reported elsewhere. Here we demonstrate the generic potential of the $Al^{18}F$-RESCA-method by labeling human serum albumin, a nanobody targeting the Kupffer cell marker CRIg, and an affibody targeting HER2 (PEP04314).

Materials and Methods

General

All reagents and solvents were purchased from Sigma-Aldrich (Bornem, Belgium), Fluka (Bornem, Belgium), Fisher (Doornik, Belgium) or Acros Organics (Geel, Belgium). The synthesis of (±)-H_3RESCA and synthesis of bifunctional derivatives is described in patent WO/2016/065435 [32]. All buffers used for derivatization and labeling of proteins were chelexed (chelex, 100 sodium form (Sigma Aldrich), 2 g/l, 30 min stirring at rt and filtration with a 0.45 µm polyamide filter (Sartorius Stedim Biotech, Göttingen, Germany)). Fluorine-18 was produced on site using a cyclotron (IBA Cyclone 18/9, IBA, Louvain-la-Neuve, Belgium) by irradiation of $H_2{}^{18}O$ with 18-MeV protons. Radioactivity was measured using an ionization chamber-based activity meter (Capintec Radioisotope Calibrator CRC-721, Ramsey, NJ, USA).

A Dionex Ultimate 3000 UPLC System (Thermo Fisher Scientific, Sunnyvale, USA) coupled in series to a UV detector, a 3-inch NaI(Tl) radioactivity detector, and an ultra-high resolution time-of-flight mass spectrometer with electron spray ionization (ESI) (MaXis Impact, Bruker, Bremen, Germany) was used for analysis of human serum albumin and nanobody constructs. For HSA, a massPREP on-line desalting cartridge (2.1 mm x 10 mm, Waters, Milford, USA) was applied using the following method. Solvent A (H_2O, 0.1% HCOOH) and solvent B (acetonitrile, 0.1% HCOOH), flow rate 0.4 ml/min. The elution gradient was: 0-1 min: 95% A; 1-3 min: from 95% A to 20% A; 3-5 min: 95% A. For nanobody constructs, a Zorbax SB-C3 column (1.8 µm, 3.0 mm x 100 mm, Agilent) was used with following gradient for (radio)-LC-HRMS: Solvent A (H_2O, 0.1% HCOOH) and solvent B (acetonitrile, 0.1% HCOOH), flow rate 0.3 ml/min. The elution gradient was: 0-1 min: 99% A; 1-7 min: from 99% A to 1% A; 7-10 min: 1% A; 10.1-12 min: 99% A. UV monitoring of the eluate was performed at 280 nm. For deconvolution analysis of the raw mass spectral data, the software program DataAnalysis (Bruker Daltonik, Bremen, Germany) was used. Calculated average neutral molecular ion mass values were obtained using Compas Isotope Pattern (version 3.2, Bruker) software.

Autoradiography was performed using phosphor storage screens (super-resolution screen, Perkin Elmer, Waltham, USA). Screens were read in a Cyclone Plus system (Perkin Elmer), and images were analyzed using Optiquant software (Perkin Elmer). Size-exclusion chromatography (SEC) was carried out with a system consisting of a Merck-Hitachi L-6200 pump and a Merck Hitachi L-4200 UV-VIS detector coupled in series to a 3-inch NaI(Tl) radioactivity detector on a Superdex 200 10/300 GL column (for HSA constructs), or on a Superdex 75 10/300 GL column (for nanobody constructs) (GE Healthcare Bio-Science AB, Uppsala, Sweden) using sodium phosphate buffer (0.01 M, pH 7.4, 0.14 M NaCl), as eluent at a flow rate of 0.5 mL/min. CRIg-deficient mice (C57Bl/6 background) were generously provided by Genentech. V4m119 nanobodies were generated and produced as described previously [33].

Synthesis of (±)-H_3RESCA-HSA

A solution of (±)-H_3RESCA-tetrafluorophenyl ester ((±)-H_3RESCA-TFP, 80 µL, 5.64 x 10^{-6} moles) in DMSO was added in a 15-molar excess to a solution of human serum albumin (1.5 ml, 3.7609 x 10^{-7} moles, CAF-DCF, Brussels, Belgium) in 0.05 M sodium bicarbonate pH 8.6, and the mixture was incubated for 2 h at rt. The conjugate was purified by gel filtration in sodium acetate buffer (0.1 M, pH 4.5, PD-10 column, GE Healthcare Bio-Science AB), and the concentration of (±)-H_3RESCA-HSA was determined spectrophotometrically at 280 nm (Nanodrop 2000, Thermo Fisher scientific). The purified product was analyzed by SEC. UV detection of the eluate was performed at 280 nm. The chelator-to-protein ratio was estimated by ESI-TOF-HRMS analysis.

Radiosynthesis and purification of (±)-[^{18}F]AlF(RESCA)-HSA

After production in a cyclotron, $[^{18}F]F^-$ was separated from $[^{18}O]H_2O$ by trapping on a SepPak Light Accel plus QMA anion exchange cartridge (Cl^- form; Waters). The cartridge was washed with water (3 mL, HPCE grade, Sigma-Aldrich), $[^{18}F]F^-$ (3.9 GBq) was eluted from the cartridge with an aqueous solution of sodium chloride 0.9% (0.3 mL, Mini-Plasco, solution for injection, B. Braun, Diegem, Belgium), and the eluate was diluted with water (0.45 mL, HPCE grade, Sigma-Aldrich). This $[^{18}F]F^-$ solution (250 µl, 1.25 GBq) was added to 25 µL of 2 mM aluminum chloride ($AlCl_3$) in sodium acetate buffer (0.1 M, pH 4.5). The solution was incubated at rt for 5 min to form $\{Al^{18}F\}^{2+}$. A solution of (±)-H_3RESCA-HSA (0.5 mL, 75 nmoles) in sodium acetate buffer (0.1 M, pH 4.5) was added to the freshly prepared $\{Al^{18}F\}^{2+}$ solution, and was incubated at room temperature (20-22 °C) for 12 min. The pH of the

final reaction mixture was checked, and was found to be pH 4.6. After incubation, the mixture was purified by gel filtration with phosphate buffered saline (PBS, 0.1 M pH 7.4, PD-10 column, GE Healthcare Bio-Science AB). Radiochemical yield was calculated based on the amount of radioactivity eluted from the column relative to the starting activity of $[^{18}F]F^-$. Radiochemical identity and purity were assessed by SEC. The identity of the main compound was confirmed using non-radioactive HSA as reference material.

Synthesis of (±)-H_3RESCA-NbV4m119

A solution of (±)-H_3RESCA-TFP (23 µl, 1.4294 x 10^{-6} moles) in DMSO was added in 12-molar excess to a solution of NbV4m119 (2.5 ml, 1.1912 x 10^{-7} moles,) in 0.05 M sodium bicarbonate pH 8.6, and the mixture was incubated for 3 h at room temperature. The conjugate was purified by gel filtration with a sodium acetate buffer (0.1 M, pH 4.5, PD-10 column, GE Healthcare Bio-Science AB), and the concentration of (±)-H_3RESCA-NbV4m119 was determined spectrophotometrically at 280 nm (Nanodrop 2000, Thermo Fisher scientific) using the corrected extinction coefficient (ε = 35,425 $M^{-1}cm^{-1}$). Analysis of the purified compound was performed by SEC. The chelator-to-protein ratio was estimated by ESI-TOF-HRMS analysis.

Radiosynthesis and semi-automated purification of (±)-[^{18}F]AlF(RESCA)-NbV4m119

$[^{18}F]F^-$ was separated from $[^{18}O]H_2O$ by trapping on a SepPak Light Accel plus QMA anion exchange cartridge (Cl^- form; Waters). The cartridge was washed with water (3 mL, HPCE grade, Sigma-Aldrich), $[^{18}F]F^-$ was eluted from the cartridge with an aqueous solution of sodium chloride 0.9% (0.3 mL, Mini-Plasco, solution for injection, B. Braun), and the eluate was diluted with water (2.7 ml, HPCE grade, Sigma-Aldrich). The $[^{18}F]F^-$ solution (0.5 ml) was added to 12.5 µL of 2 mM aluminum chloride ($AlCl_3$) in sodium acetate buffer (0.1 M, pH 4.5). The solution was incubated at rt for 5 min to form $\{Al^{18}F\}^{2+}$. A solution of (±)-H_3RESCA-NbV4m119 (1.5 mL, 0.55 mg/ml) in sodium acetate buffer (0.1 M, pH 4.5) was added to the freshly prepared $\{Al^{18}F\}^{2+}$ solution and the mixture was incubated at ambient temperature (20-22 °C) for 12 min. After incubation, the mixture was purified using four Hitrap desalting columns in series (GE Healthcare Bio-Science AB) using sodium phosphate buffer (0.01 M, pH 7.4, 0.14 M NaCl) as eluent at a flow rate of 1 mL/min. A UV detector and 3-inch NaI(Tl) radioactivity detector were coupled in series to be able to collect the purified product and to calculate the radiochemical yield. The collected fraction was filtered through a 0.22-µm filter (Millex-GV, 13 mm, Merck KGaA, Darmstadt, Germany), and diluted with sodium phosphate buffer (0.01 M, pH 7.4, 0.14 M NaCl). Radiochemical identity and purity were assessed by SEC and by radio-LC-HRMS. The identity of the main compound was confirmed using unlabeled NbV4m119 as reference material.

In vitro stability studies

A volume of 100 µL of purified (±)-[^{18}F]AlF(RESCA)-HSA (22 MBq) or (±)-[^{18}F]AlF(RESCA)-NbV4m119 (24 MBq) was added to freshly isolated rat plasma (1 mL). The mixtures were incubated at 37 °C and analysed at 1, 2, 3, and 4 h after the start of incubation by SEC.

Biodistribution and microPET studies with (±)-[^{18}F]AlF(RESCA)-HSA and (±)-[^{18}F]AlF(RESCA)-NbV4m119

Quantification of radioactivity for biodistribution studies was performed using an automated gamma counter equipped with a 3-inch NaI(Tl) well crystal coupled to a multichannel analyser, mounted in a sample changer (Perkin Elmer 1480 Wizard 3q). Counts were corrected for background radiation, physical decay and counter dead time. Animals were housed in individually ventilated cages in a thermo-regulated (~22 °C), humidity-controlled facility under a 12h-12h light-dark cycle, with access to food and water *ad libitum*. All animal experiments were conducted according to the Belgian code of practice for the care and the use of animals, after approval from the university animal ethics committee.

The biodistribution study of (±)-[^{18}F]AlF (RESCA)-HSA was carried out in healthy female Wistar rats (body weight: 187-225 g) at 1 h, 3 h, and 6 h post injection (p.i.; n = 4/time point). Rats were injected with (±)-[^{18}F]AlF(RESCA)-HSA (2-7.5 MBq, 17-62 µg) *via* a tail vein under anesthesia (2.5% isoflurane in O_2 at 1 L/min flow rate), and sacrificed by decapitation at above specified time points. The biodistribution study of (±)-[^{18}F]AlF(RESCA)-NbV4m119 was carried out in healthy male C57BL/6 mice (body weight: 22-26 g) at 1 h and 3 h p.i. (n = 3/time point) or in CRIg-deficient mice ($CRIg^{-/-}$, C57BL/6 background, body weight: 20-23 g) at 3 h p.i. (n = 3/time point). Mice were injected with freshly filtered (0.22 µm, Millipore) (±)-[^{18}F]AlF(RESCA)-NbV4m119 (7-11 MBq, 8-13 µg) *via* a tail vein under anesthesia (2.5% isoflurane in O_2 at 1 L/min flow rate), and sacrificed by decapitation at above specified time points. Blood and major organs were collected in

tared tubes and weighed. The radioactivity in blood, organs, and other body parts was counted using an automated γ-counter. Results are presented as standardized uptake values (SUV; tissue activity (MBq/g)/[injected dose (MBq)/body weight (g)]).

Small animal whole-body PET imaging was performed using a FOCUS™ 220 microPET scanner (Concorde Microsystems, Knoxville, US), and PMOD software (v 3.2, PMOD Technologies, Zürich, Switzerland) was used to analyze the images. The animals were kept under gas anaesthesia during the entire procedure (2.5% isoflurane in O_2 at 1 L/min flow rate). A whole-body PET image of a healthy rat was obtained 180 min after intravenous injection of (±)-[^{18}F]AlF(RESCA)-HSA (96 MBq, 798 µg). A 60-min dynamic microPET scan was performed on a healthy male C57BL/6 mouse (body weight: 24 g) and CRIg-deficient mouse (CRIg$^{-/-}$, C57BL/6 background, body weight: 23 g) simultaneously. The scan was started immediately after intravenous injection of sterile filtered (0.22 µm, Millipore) (±)-[^{18}F]AlF(RESCA)-NbV4m119 (11 MBq, 13 µg).

Synthesis of (±)-H_3RESCA-PEP04314 and H_2NOTA-PEP04314

Five mg of lyophilized PEP04314 (0.71 µmol, Affibody AB, Solna, Sweden) was added to 0.5 mL of 0.2 M ammonium acetate buffer (pH 7.5), and the solution was added to a reaction vial containing 0.4 mg (0.72 µmol) of (±)-H_3RESCA-maleimide or maleimide-mono-amide-NOTA (Macrocyclics, Plano, Tx, USA). The reaction mixture was kept at room temperature for 90 min before being transferred to an ultracel 3K centrifugal filter (Merck) containing 3 mL of 0.1 M ammonium acetate buffer (pH 4) and centrifuged at 4000 rpm for 90 min. The flow-through was discarded, and 4 mL of fresh 0.1 M ammonium acetate buffer (pH 4) was added. The filter was then centrifuged again for 90 min, and the flow-through was discarded. Purified (±)-H_3RESCA-PEP04314 or H_2NOTA-PEP04314 was collected *via* reverse spin in 1 mL of 0.1 M ammonium acetate buffer (pH 4.5), and stored at -70 °C in 100 µL aliquots prior to use. Purity of the final product was determined *via* a Waters Acquity LC/MS system equipped with a Waters Xselect CSH C18 column (250 mm ×10 mm, 130 Å) at a flow rate of 5 mL/min using a gradient of EtOH (10-40% over 15 min) and 0.1% formic acid.

Radiosynthesis (±)-[^{18}F]AlF(RESCA)-PEP04314 and [^{18}F]AlF(NOTA)-PEP04314

A SepPak Light Accel plus QMA anion exchange cartridge (HCO_3^- form; Waters) containing [^{18}F]-fluoride was first washed with 1.5 mL of ultrapure water (Water Ultra Trace Elemental Analysis Grade, Fisher Chemical, Pittsburgh, USA), and then [^{18}F]-fluoride was eluted with 1.0 mL of 0.4 M $KHCO_3$. An aliquot of 100 µL of the eluted [^{18}F]-fluoride solution was added to a reaction vial containing 10 µL acetic acid, 50 µL $AlCl_3$ solution (2 mM in 0.1 M NaOAc buffer, pH 4), and 125 µL 0.1 M NaOAc pH 4. The solution was incubated for 2 min at room temperature prior to addition of 0.5 mg (±)-H_3RESCA-PEP04314 or H_2NOTA-PEP04314 in 400 µL of a 1:1 solution of ethanol and 0.1 M NaOAc pH 4. The reaction mixture was heated for 15 min at 37 °C for (±)-H_3RESCA-PEP04314 and at 100 °C for H_2NOTA-PEP04314. After heating, the reaction mixture was transferred to a vial containing 0.7 mL of 0.1% formic acid, and mixed and purified by HPLC on a Waters Xselect CSH C18 column (250 mm ×10 mm, 130 Å) at a flow rate of 5 mL/min using a gradient of EtOH (10-40% over 15 min) and 0.1% formic acid. The peak corresponding to (±)-[^{18}F]AlF(RESCA)-PEP04314 or [^{18}F]AlF(NOTA)-PEP04314 was collected and transferred to a sterile vial using normal saline as a rinse to give (±)-[^{18}F]AlF(RESCA)-PEP04314 or [^{18}F]AlF(NOTA)-PEP04314**.** Specific activity and radiochemical purity were determined via a Waters Acquity LC/MS system on a Waters Xselect CSH C18 column (250 mm ×10 mm, 130 Å) at a flow rate of 5 mL/min using a gradient of EtOH (10-40% over 15 min) and 0.1% formic acid and a *β*-RAM Model 4 radio-HPLC detector (IN/US Systems, Brandon, FL, USA).

PET/CT studies with (±)-[^{18}F]AlF(RESCA)-PEP04314 and [^{18}F]AlF(NOTA)-PEP04314 in non-human primates

PET studies were conducted in healthy adult rhesus monkeys (n=4, rhesus monkey A-D, weight 7.6 ± 1.8 kg). All procedures were conducted in accordance with the guidelines of the Institutional Animal Care and Use Committee of Merck (West Point, PA) and guidelines for the care and use of mammals in neuroscience and behavioral research (National Research Council 2003). Animals were housed in temperature- and humidity-controlled rooms in fully AAALAC (Association for Assessment and Accreditation of Laboratory Animal Care) accredited facilities and fed a commercially prepared high protein monkey diet (Lab Diet no. 5045, PMI Nutrition International, Brentwood, MO); water was offered ad libitum. Fresh fruits and vegetables were provided daily and animal housing rooms were maintained on a twelve hour light/dark cycle.

Animals were fasted and initially anesthetized with ketamine (10 mg/kg IM), and then maintained

under anesthesia using IV propofol (5 mg/kg induction, 0.6 mg/kg/min maintenance). Following the initial induction with propofol, the animal was intubated and ventilated with medical grade compressed air at ~10 mL/breath/kg and 23 respirations per minute. Monkeys were instrumented with a temperature probe, a pulse oximeter and an end tidal CO_2 monitor. End tidal CO_2 was maintained at 40 ± 2 mm Hg, with body temperature maintained between 37–38 °C using a T-pump warming pump (Gaymar Industrial, Orchard Park, NY) with K-module heating pads (Harvard Apparatus, Holliston, MA)

PET data were acquired on a Siemens Biograph 64 TruePoint PET/CT scanner (Siemens Medical Solutions, Malvern, PA).The PET scanner was cross-calibrated with the dose calibrator using an ^{18}F cylinder according to the manufacturer's standard operating procedures. Following a whole body CT scan used to correct for photon attenuation and scatter, 29-149 MBq (9-48 µg) of (±)-[^{18}F]AlF(RESCA)-PEP04314 (n=3; n=1 in rhesus monkey A, n=1 in rhesus monkey B, n=1 in rhesus monkey C) or [^{18}F]AlF(NOTA)-PEP04314 (n=6; n=2 in rhesus monkey A, n=2 in rhesus monkey B, n=2 in rhesus monkey D) was injected as a 2-min bolus IV. A whole body dynamic emission scan was acquired for 180 minutes, encompassing five fields of view (24 static frames). Venous samples to measure blood levels of radiotracer were obtained throughout the scan. Following PET data acquisition, a whole body CT with contrast (~3 ml Omnipaque/kg) was obtained.

PET data were reconstructed using the vendor-suppled iterative method with 4 iterations and 8 subsets. CT-based attenuation and scatter correction were carried out as implemented by the camera manufacturer. Regions of Interest (ROIs) were drawn for liver, kidney cortex, heart blood pool, salivary glands, bladder, lung, and muscle using both the PET and CT images to guide ROI placement, and time activity curves (TACs) were calculated. Bone ROIs were drawn on the lumbar spine. Results are presented as standardized uptake values (SUV; tissue activity (MBq/cm^3)/[injected dose (MBq)/body weight (g)]). Additional ROIs were drawn to encompass all of the bladder and kidney, and these were compared to the total radioactivity measured in the image to calculate the percentage injected dose (%ID) for each organ. Radiotracer levels in venous blood samples were fit to a bi-exponential clearance curve, and alpha and beta clearance half-lives in blood were estimated.

Statistical analysis

Quantitative data are expressed as mean ± standard deviation (STDEV) unless stated otherwise. Means were compared using the unpaired two-tailed Student t-test. Values were considered statistically significant for $P < 0.05$.

Results and Discussion

(±)-[^{18}F]AlF(RESCA)-Human serum albumin

The best method to assess the *in vivo* stability of a chelate is to attach it to a suitable vector that is slowly cleared from plasma and thus remains in circulation for an extended period of time. Human serum albumin (HSA, 66.5 kDa) is a heat-sensitive globular protein (melting temperature, T_m, of 71°C at 0.5 mg/ml) [34] with a primary sequence made up of 585 amino acid residues, and is the most abundant protein in human plasma (3.5-5 g/dL) [35]. It accounts for about 70% of the plasma colloid osmotic pressure. Its high solubility, stability and plasma half-life of approximately 16-18 h make HSA the ideal vector to evaluate the stability of the Al^{18}F-chelate *in vivo*. Moreover, the Al^{18}F-labeled construct can potentially be used for PET blood pool imaging applications [36].

HSA possesses 59 lysine residues that can be used for the introduction of chelators via reaction of ε-amino groups with an excess of (±)-H_3RESCA-TFP (**Figure S1**). (±)-H_3RESCA-TFP ester was efficiently conjugated to HSA providing (±)-H_3RESCA-HSA with a chelator-to-protein ratio of 3, estimated by ESI-TOF-HRMS analysis, and no aggregates or degradation products were detected (**Figure S2**). (±)-H_3RESCA-HSA was labeled directly with [^{18}F]{AlF}$^{2+}$ and a good radiochemical yield (RCY 52-63%) was achieved using mild reaction conditions (rt, 12 min, pH 4.6) compatible with the structural and functional integrity of proteins. (±)-[^{18}F]AlF(RESCA)-HSA was purified using a disposable size-exclusion cartridge, providing the final product in high radiochemical purity, as assessed by size-exclusion chromatography (**Figure 2**).

This method provided higher radiochemical yields in considerably shorter overall synthesis time than other radiofluorination strategies such as the prosthetic group approach using [^{18}F]F-Py-TFP described by Basuli *et al.* [36] and the Cu(I)mediated 1,3-dipolar [3+2]cycloaddition reaction reported by Ramenda *et al.* [37] (**Table 1**). (±)-[^{18}F]AlF(RESCA)--HSA showed excellent stability *in vitro*. After 4 h incubation in rat plasma at 37 °C, 92% of the Al^{18}F-tracer was still intact as assessed by size exclusion chromatography (**Figure S3**).

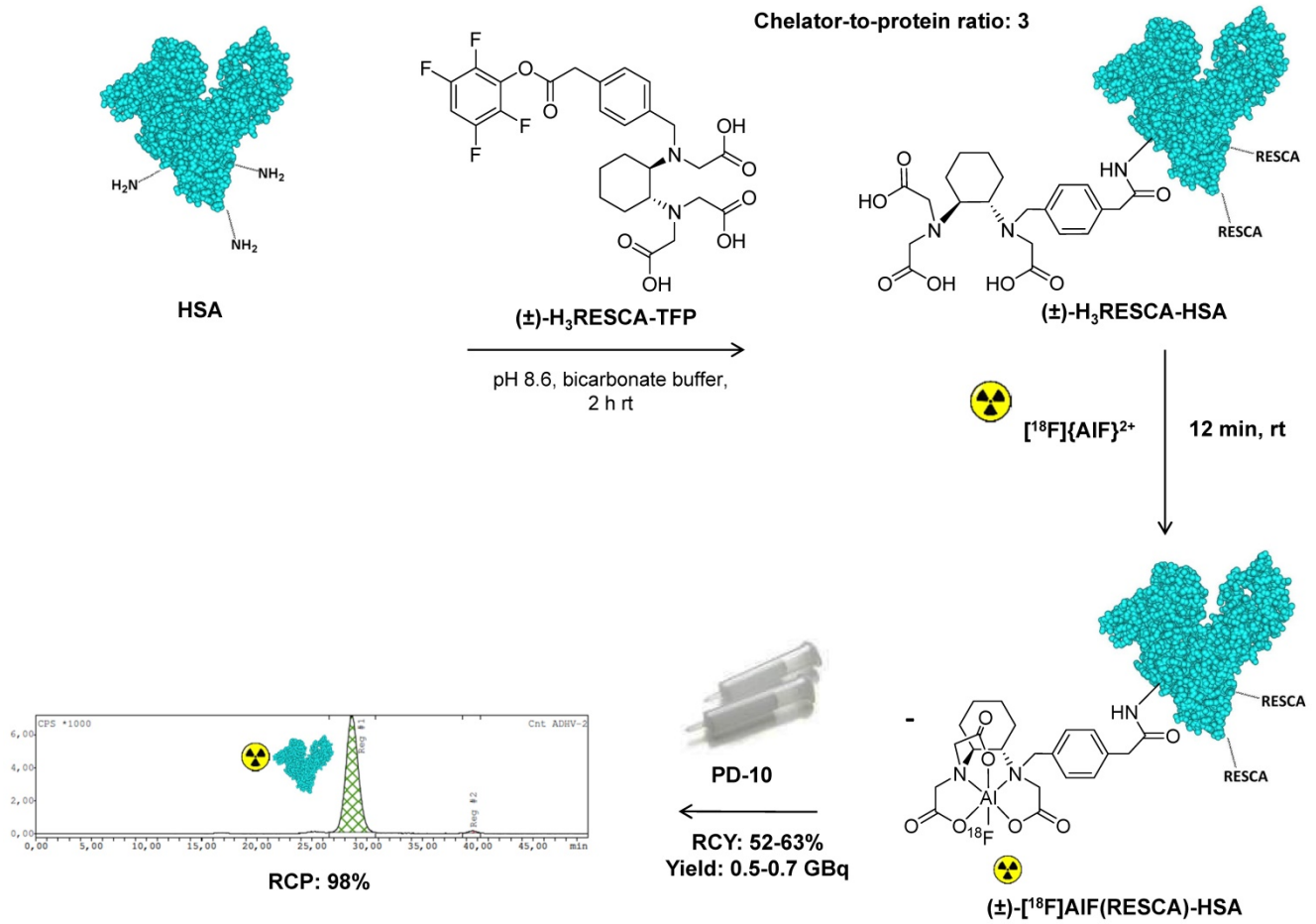

Figure 2. Synthesis and radiolabeling of (±)-H3RESCA-HSA with [18F]{AlF}2+. (±)-H3RESCA-TFP ester was conjugated to HSA providing (±)-H3RESCA-HSA. (±)-[18F]AlF(RESCA)-HSA was prepared in high RCY and RCP, as assessed by size-exclusion chromatography (SEC), in less than 30 min (starting after elution of fluorine-18 from the anion exchange QMA cartridge). SEC-radio-chromatogram of purified (±)-[18F]AlF(RESCA)-HSA with a retention time of 28.5 min. HSA = human serum albumin (PDB ID:1E7H), rt = room temperature (20-25°C), RCY = radiochemical yield (calculated based on the amount of radioactivity eluted from disposable desalting column relative to the starting activity of [18F]F−), RCP = radiochemical purity.

Table 1. Comparison of different radiofluorination methods for labeling the heat-sensitive protein HSA.

Method	(±)-[18F]AlF(RESCA)-HSA	[18F]F-Py-HSA [36]	Cu(I)mediated 1,3-dipolar [3+2]cycloaddition [37]
RCY*	52-63% (n=3)	18-35% (n=30)	15-20%
RCP	> 98%	> 98%	> 95%
Synthesis time**	< 30 min	90 min	120 min
Tb	8.6 h (in rats)	4.8 h# (in rats)	31 min (in mice)

RCY: radiochemical yield; RCP: radiochemical purity; Tb: blood biological half-life
*Calculated based on the amount of radioactivity eluted from disposable desalting column relative to the starting activity of [18F]F-**Starting from [18F]F- # Data for [18F]F-Py-RSA (rat serum albumin)

Biodistribution of (±)-[18F]AlF(RESCA)-HSA in rats showed high retention in blood with SUV: 11.8 ± 0.6, 10.1 ± 0.7, and 8.0 ± 0.1 at 1 h, 3 h, and 6 h, respectively (**Figure 3A, Table S1**). Blood data points were fitted with a one- component exponential equation ($y = 12.75e^{(-0.08x)}$; $R^2 = 0.9998$), from which the blood biological half-life (Tb) was calculated to be 8.7 h (**Figure S4**). This indicates that the introduction of RESCA residues into HSA and subsequent radiolabeling using the Al18F-method did not alter the structural and functional integrity of HSA. In contrast, the radiolabeling method using a Cu(I)mediated 1,3-dipolar [3+2]cycloaddition significantly affected functional integrity of HSA, resulting in a Tb of only 31 minutes [37]. Fluorine-18 in the form of fluoride and also [18F]{AlF}2+ are known to accumulate in bone [38, 39]. Bone is a highly vascular tissue [40], so this might explain the observed bone uptake at 1 h p.i. However, only minor increase in bone uptake was observed over time, indicating high *in vivo* stability of the Al18F-labeled protein conjugate. Moreover, (±)-[18F]AlF(RESCA)-HSA showed favorable properties for PET blood pool imaging applications. A whole body PET image of a healthy rat 180 min after intravenous injection of (±)-[18F]AlF(RESCA)-HSA is shown in **Figure 3B.** The ventricles of the heart and the peripheral vasculature are well visualized. Other organs can be observed but retain lower

concentrations of fluorine-18 than the central vasculature. The tissue concentrations in the microPET study are consistent with the *ex vivo* biodistribution results at comparable time points.

(±)-[^{18}F]AlF(RESCA)-Nanobody

Nanobodies (Nb, V_{HH}) are heat-sensitive antigen-binding fragments derived from heavy-chain-only antibodies occurring naturally in Camelid species and can be considered as *magic bullets* for immuno-PET imaging [41]. Nanobodies bind their antigens very fast and specifically with high affinity *in vivo*, whereas unbound nanobody is rapidly cleared from blood by the kidneys [42]. Using nanobodies labeled with a positron emitting radionuclide, high contrast PET images can be acquired as early as 1 hour after tracer administration [43]. This early imaging allows the use of short-lived PET radionuclides such as fluorine-18. Xavier *et al.* recently reported successful ^{18}F-labeling of HER2-targeting nanobodies using the prosthetic group [^{18}F]SFB [44]. The same method was used by Blykers *et al.* and Bala *et al.* for radiofluorination of nanobodies targeting the macrophage mannose receptor (MMR) [45] and the vascular cell adhesion molecule (VCAM1) [46], respectively.

However, this multistep synthesis is laborious, and only limited yields of purified radiolabeled product were obtained with moderate apparent molar radioactivity **(Table 2)**. We have evaluated the Al^{18}F-method for radiolabeling of the nanobody NbV4m119 [47], targeting the complement receptor of the Ig superfamily (CRIg) [48]. CRIg has a pronounced expression on Kupffer cells, which are resident liver macrophages. Moreover, it has been shown that CRIg is more abundant in rheumatoid arthritis (RA) synovial tissue than in normal synovium [33]. Consequently, CRIg is a promising marker to monitor changes in Kupffer cell dynamics [49] and for specific molecular imaging of RA, allowing non-invasive quantification of joint inflammation [33].

Characterization of a radiolabeled nanobody is important in order to confirm that the derivatization and radiolabeling procedure does not affect the nanobody integrity. We have therefore explored radio-liquid chromatography in combination with high-resolution mass spectrometry (radio-LC-HRMS) to analyze NbV4m119 before and after derivatization with (±)-H_3RESCA-TFP ester. The theoretical average neutral molecular mass ([M]) of unlabeled NbV4m119 is 14577.85 Da [M] (calculated for $C_{643}H_{950}N_{188}O_{196}S_4$), and the observed molecular mass after deconvolution was 14577.61 ± 0.02 Da [M] (**Figure S5**). We also observed the presence of a deamination product with an observed molecular mass of 14560.76 ± 0.02 Da (calculated for $C_{643}H_{947}N_{187}O_{196}S_4$ [M]: 14560.82). This deamination product was expected and can be formed spontaneously during manipulation and storage of the protein.

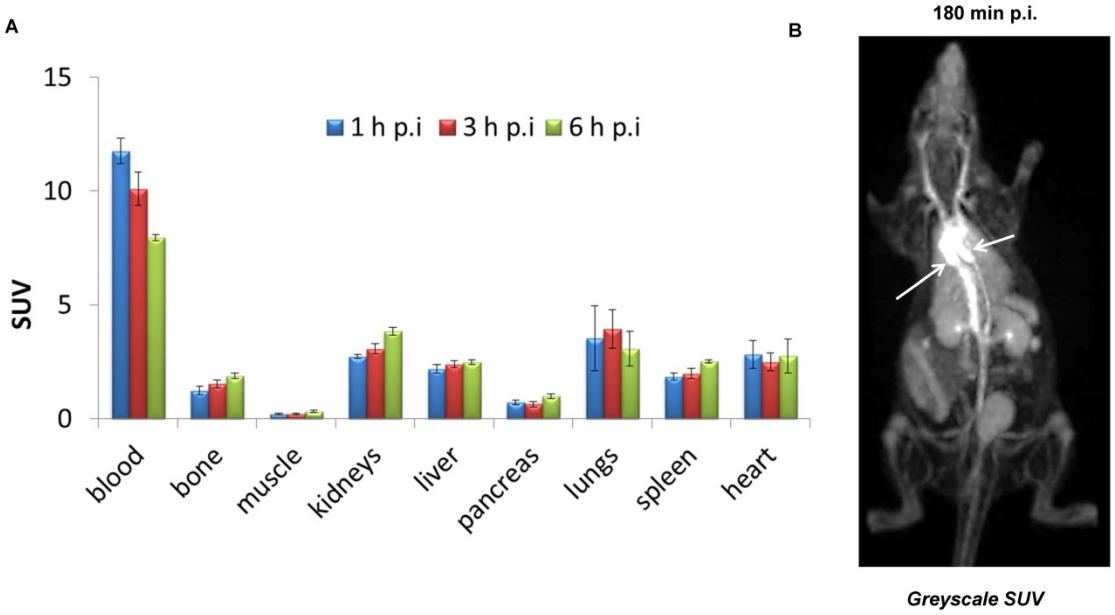

Figure 3. Biodistribution and PET imaging of rats after intravenous injection of (±)-[^{18}F]AlF(RESCA)-HSA. Biodistribution **(A)** of (±)-[^{18}F]AlF(RESCA)-HSA in rats at 1 h, 3 h, and 6 h p.i. (n=4/group) and whole-body PET image **(B)** of a healthy rat 180 min after intravenous injection of (±)-[^{18}F]AlF(RESCA)-HSA (greyscale SUV (g/ml): max, white; min, black) White arrows indicate ventricles of the heart. Results of biodistribution are presented as standardized uptake values (SUV; tissue activity (MBq/g)/[injected dose (MBq)/body weight (g)]). Blood data points were fitted with a one- component exponential equation: $y = 12.75e^{(-0.08x)}$; $R^2 = 0.9998$, blood biological half-life (Tb) = 8.66 h.

Table 2. Comparison of two radiofluorination methods for labeling of nanobodies

Method	Al^{18}F-RESCA	[^{18}F]SFB [44]	[^{18}F]SFB [45]	[^{18}F]SFB [46]
Target	CRIg	HER2	MMR	VCAM-1
Nanobody	V4m119	2Rs15d	3.49 sdAb	cAbVCAM-1–5
RCY	35-53%* (n=3)	5-15%** (n=3)	5-15%**	/
RCP	> 98%	> 98%	> 97%	> 99%
Synthesis time#	< 35 min	180 min	180 min	180 min
GBq/μmol ##	80-85	17-33	10-30	/
Overall batch activity	2-2.2 GBq	0.2- 0.5 GBq	/	/

RCY: radiochemical yield; RCP: radiochemical purity

*Calculated based on the preparative chromatogram and relative to radioactivity of [^{18}F]F$^-$/[^{18}F]{AlF}$^{2+}$ **Calculated based on the amount of radioactivity eluted from disposable desalting column relative to the starting activity of [^{18}F]F$^-$ #Starting from [^{18}F]F$^-$ ##Apparent molar radioactivity at the end of purification

NbV4m119 possesses five lysine residues in its amino acid sequence, therefore several lysine groups can react with the (±)-H$_3$RESCA-TFP active ester *via* the free amino functionalities (**Figure S6**). (±)-H$_3$RESCA-TFP ester was efficiently conjugated to NbV4m119 providing (±)-H$_3$RESCA-NbV4m119 with a chelator-to-protein ratio of 1.5, estimated by ESI-TOF-HRMS analysis, and no aggregates or degradation products were observed (**Figure S7**). The theoretical average neutral molecular masses for single and dual conjugation are 14979.26 Da [M] (calculated for $C_{664}H_{973}N_{189}O_{203}S_4$) and 15397.70 Da [M] (calculated for $C_{685}H_{999}N_{191}O_{210}S_4$), respectively. The observed molecular masses for (±)-H$_3$RESCA-NbV4m119 after deconvolution were 14979.35 ± 0.02 Da and 15397.69 ± 0.02 Da [M], respectively.

(±)-H$_3$RESCA-NbV4m119 was labeled with [^{18}F]{AlF}$^{2+}$, achieving good radiochemical yields using mild conditions and the crude reaction mixture was purified using four Hitrap desalting columns in series yielding the purified batch (±)-[^{18}F]AlF (RESCA)-NbV4m119 (**Table 2** and **Figure 4**). (±)-[^{18}F]AlF(RESCA)-NbV4m119 was analyzed with radio-RPLC-HRMS and SEC, eluting at a retention time of 5.6 min and 26.9 min, respectively (**Figure S8** and **Figure 4**) to check the radiochemical purity of the radiolabeled nanobody. No aggregation or degradation products were observed. The radiofluorination method provided higher radiochemical yields, higher overall batch activity and higher apparent molar radioactivity in considerably shorter overall synthesis time than the prosthetic group approach using [^{18}F]SFB (**Table 2**). Analysis with SEC revealed that 96% of the Al^{18}F-tracer was still intact after 6 h incubation in the storage buffer (**Figure S9**), and 91.5% of the Al^{18}F-tracer was still intact after 3 h incubation in rat plasma at 37 °C, indicating excellent *in vitro* stability of (±)-[^{18}F]AlF(RESCA)-NbV4m119 (**Figure S10**).

Since the molecular size of nanobodies is below the threshold for renal glomerular filtration (<60 kDa), nanobodies are generally cleared quickly from blood, primarily *via* renal clearance. Only 0.20 ± 0.02 and 0.13 ± 0.02 SUV of the radioactivity was observed in blood after 1 h and 3 h p.i. respectively, indicating fast blood clearance (**Table S2**). It is known that nanobodies are efficiently reabsorbed in the renal proximal tubuli, and Gainkam *et al*. showed elegantly that the megalin receptor plays an important role in this mechanism using megalin-knockout mice [50]. Kidney retention is also significantly affected by the presence of a hexahistidine tag, which is genetically inserted in the structure of NbV4m119 for the purpose of immobilized metal ion affinity chromatography purification [50].

As expected, high uptake in kidneys (SUV: 37.6 ± 4.5) was observed at 1 h p.i. **Figure S11** shows an *ex vivo* autoradiogram of a renal tissue slice of a naive WT mouse injected with (±)-[^{18}F]AlF(RESCA)-NbV4m119 and sacrificed at 1 h p.i. The radioactivity is mainly concentrated in the renal cortex indicating that the kidney retention may be caused by tubular reabsorption and subsequent internalization. Remarkably, at 3 h p.i. kidney uptake was decreased drastically (SUV: 8.9 ± 2.3) with a corresponding fraction being excreted with the urine, strongly indicating that resulting (radio)catabolites are non-residualizing. Urine analysis shows the presence of mainly radiometabolites of (±)-[^{18}F]AlF(RESCA)-NbV4m119, confirming the hypothesis of renal metabolism followed by elimination of the catabolites *via* the urine (**Figure S12-S13**). This high rate of *in vivo* degradation was also reported previously for ^{99m}Tc-labeled nanobodies targeting the epidermal growth factor receptor (EGFR). In this study the authors found that only 10% of ^{99m}Tc-labeled nanobody in urine was intact at 1 h p.i. indicating that this degradation is specific for nanobodies rather than dependent on the radiolabeling method [50].

Zheng *et al.* investigated CRIg mRNA levels in collagen-induced arthritis (CIA) mice to determine whether this marker is expressed homogeneously in the body or specifically in certain tissues during inflammation [33]. High CRIg mRNA levels were found in liver (the CRIg receptor has a pronounced

expression on CD11b^{intermediate} F4/801 Kupffer cells in the liver) and low or undetectable quantities in bone marrow, lymph nodes, spleen and lungs. In accordance with these results (±)-[^{18}F]AlF(RESCA)-NbV4m119 showed high uptake in liver (SUV: 2.3 ± 0.2, liver-to-muscle ratio of 33 ± 2.1) at 3 h p.i. in healthy mice, but low uptake in other organs (**Figure 5A**). In CRIg$^{-/-}$ mice no specific uptake of (±)-[^{18}F]AlF(RESCA)-NbV4m119 could be observed in the liver (SUV: 0.27 ± 0.1, $P < 0.001$) at 3 h p.i., indicating excellent *in vivo* CRIg specificity of the tracer. This demonstrates that the Al^{18}F-RESCA labeling method does not affect the functional integrity of nanobodies.

Higher kidney uptake in the CRIg$^{-/-}$ mice at 3 h p.i compared with the kidney uptake in the WT mice at 3 h p.i. ($P < 0.005$) may be explained by the lower liver uptake in CRIg$^{-/-}$ mice, resulting in higher availability of [^{18}F]AlF-RESCA-NbV4m119 towards the renal elimination pathway. It is important to minimize residence time of (±)-[^{18}F]AlF(RESCA)-NbV4m119 in plastic syringes to avoid aggregation, which might result in increased lung uptake. Probably, aggregation over time in these syringes explains the relative high variation in lung uptake seen in the biodistribution study. Aggregation of proteins is a common problem and might be related to this specific nanobody or labeling method. To overcome this issue, different agents can be added to the final formulation buffer that promote protein solubility (e.g. 0.1% w/v polysorbate 80) [51].

Although we showed excellent *in vitro* stability of (±)-[^{18}F]AlF(RESCA)-NbV4m119 in rat plasma, the biodistribution study showed an increase of bone uptake over time, indicating minor levels of demetallation and/or defluorination of the compound (SUV: 0.6 ± 0.1 and 1.0 ± 0.3 at 1 h and 3 h p.i., respectively). One should consider the harsh environment in kidney lysosomes as a possible explanation for the observed elevated bone uptake. Indeed, after glomerular filtration, nanobodies are internalized and transported to lysosomes [50]. Here, (±)-[^{18}F]AlF(RESCA) may be degraded, and as a result [^{18}F]{AlF}$^{2+}$ and/or [^{18}F]F$^-$ could be recycled back into circulation, resulting in increased bone uptake values. Non-specific bone accumulation might compromise the utility of this tracer for noninvasive quantification of joint inflammation *in vivo*.

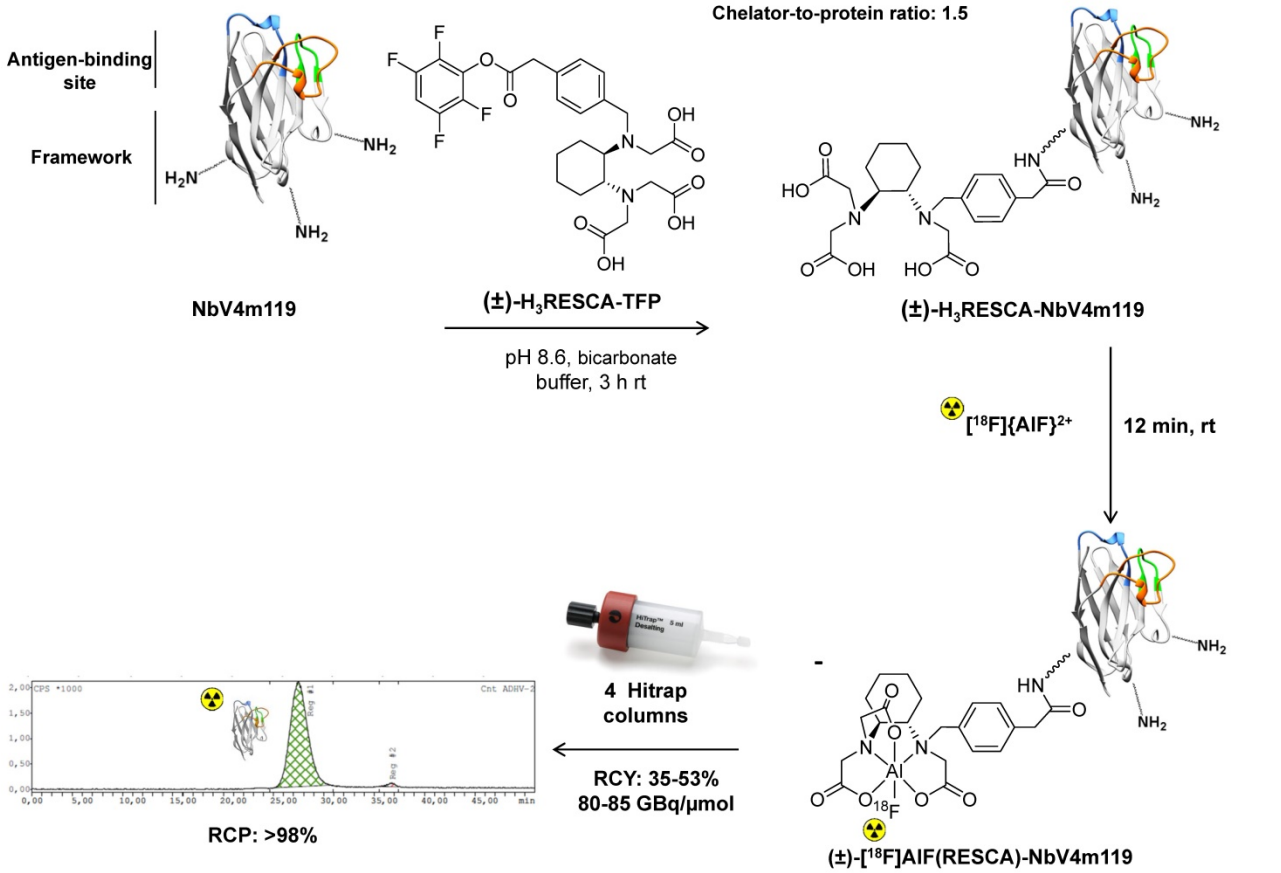

Figure 4. Synthesis and radiolabeling of (±)-H$_3$RESCA-NbV4m119 with [^{18}F]{AlF}$^{2+}$. (±)-H$_3$RESCA-TFP ester was conjugated to NbV4m119 providing (±)-H$_3$RESCA-NbV4m119. (±)-[^{18}F]AlF(RESCA)-NbV4m119 was prepared in high radiochemical yield. Purification was accomplished with SEC using 4 Hitrap desalting columns in series, affording highly pure (±)-[^{18}F]AlF(RESCA)-NbV4m119 in less than 35 min (starting after elution of fluorine-18 from the anion exchange QMA cartridge). SEC Radio-chromatogram of purified (±)-[^{18}F]AlF(RESCA)-NbV4m119 eluting with a retention time of 26.9 min. rt = room temperature (20-25 °C), RCY = radiochemical yield (calculated based on the preparative chromatogram and relative to radioactivity of [^{18}F]F$^-$/[^{18}F]{AlF}$^{2+}$), RCP = radiochemical purity.

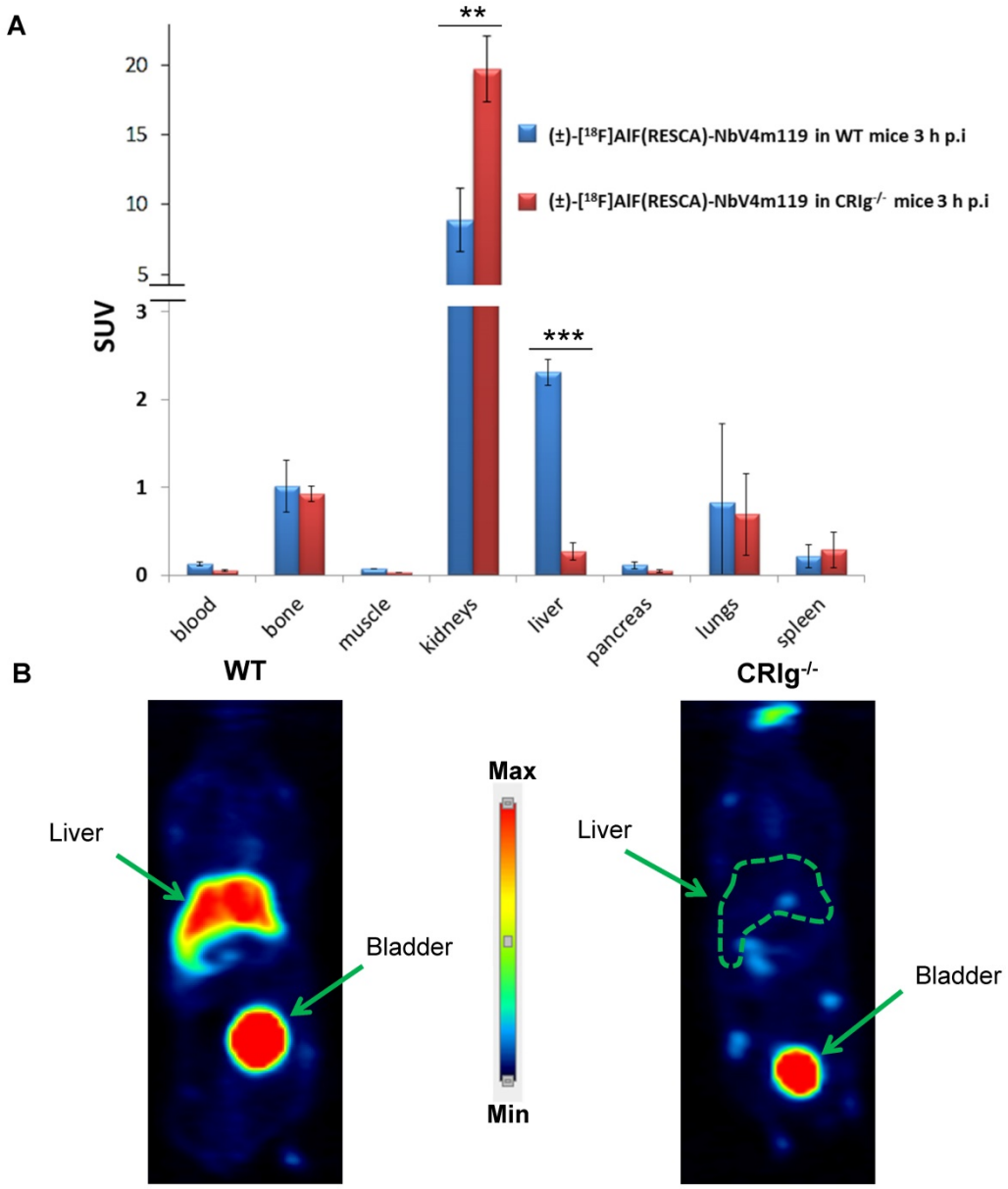

Figure 5. Biodistribution and PET imaging of WT and CRIg$^{-/-}$ mice after intravenous injection of (±)-[^{18}F]AlF(RESCA)-NbV4m119 A: Biodistribution of (±)-[^{18}F]AlF(RESCA)-NbV4m119 in wild-type mice (WT) and CRIg$^{-/-}$ mice (CRIg$^{-/-}$) at 3 h p.i (n=3/group). Biodistribution results are presented as standardized uptake value (SUV; tissue activity (MBq/g)/[injected dose (MBq)/body weight (g)]). **P < 0.005***P < 0.001 **B:** Coronal microPET images. Summed images (30-60 min p.i., time weighted average) performed on naive WT and CRIg$^{-/-}$ mice.

Nevertheless, the calculated bone uptake is limited and might be species-dependent. Whole-body PET imaging clearly showed specific uptake of (±)-[^{18}F]AlF(RESCA)-NbV4m119 in the liver, whereas no liver uptake was observed in the CRIg knockout mice, confirming high specificity for CRIg (**Figure 5B**). *In vivo* PET imaging did not show major bone uptake after 1 h and high liver-to background images were obtained, indicating favorable *in vivo* imaging properties of (±)-[^{18}F]AlF(RESCA)-NbV4m119.

[^{18}F]AlF-RESCA-Affibody

Affibody molecules are non-immunoglobulin--based scaffold proteins characterized by high target specificity and binding affinity (Kd in the low-nanomolar to picomolar range) [52, 53]. These small proteins have been generated against different cancer-associated molecular targets and have been labeled with different radionuclides (^{68}Ga, ^{18}F, ^{64}Cu, ^{99m}Tc, and ^{111}In) suitable for immuno-PET and SPECT [54-59]. As for nanobodies, the half-life of fluorine-18 perfectly matches the fast pharmacokinetics of affibody molecules [60]. Indeed, the small size of fluorine-18 labeled affibody molecules is responsible for fast clearance, providing high contrast images within one to three hours after injection. Furthermore, introduction of an unpaired cysteine residue at the

c-terminus of the protein allows site-specific conjugation of chelators or radiolabeled groups *via* maleimide-thiol reactions, avoiding heterogeneous tracer populations.

To show the feasibility of radiolabeling affibody molecules using the Al^{18}F-RESCA method, and to further investigate the *in vivo* stability of the (±)-[^{18}F]AlF(RESCA)-complex, we radiolabeled a generic affibody and conducted PET/CT studies in healthy non-human primates. In general, affibodies are considered to be heat-stable. However, Da Pieve *et al.* labeled a NOTA-derivatized affibody targeting HER3 with [^{18}F]AlF using standard one-pot-reaction conditions (pH 4, 100 °C for 15 min) [29]. The reported radiochemical conversion and the apparent molar radioactivity of the radioconjugate were 38.8 ± 5.8% (non-decay corrected) and 6.0−11.9 GBq/µmol, respectively. Unfortunately, thermal degradation of the radioconjugate was observed, compromising the final yield of the reaction. As shown by Heskamp *et al*., good to excellent yields can also be obtained at 90°C for labeling of affibodies that are more sensitive [61]. Nevertheless, direct radiolabeling at low temperature (<40°C) using the Al^{18}F-RESCA method could provide an interesting alternative to avoid possible thermal degradation.

As a proof of concept, we successfully derivatized affibody molecules (PEP04314, also known as $Z_{HER2:2891}$) targeting HER2, exploiting site-specific maleimide-thiol reactions with (±)-H_3RESCA-maleimide to afford (±)-H_3RESCA-PEP04314. As a control, we also derivatized affibody molecules site-specifically with maleimide-mono-amide-NOTA to afford H_2NOTA-PEP04314. The purity of the final products was determined with LC/MS (**Figure S14**). (±)-H_3RESCA-PEP04314 and H_2NOTA-PEP04314 were labeled with [^{18}F]{AlF}$^{2+}$ in radiochemical yields of respectively 20 ± 7% (n=4) and 8 ± 6% (n=4). Labeling conditions for both compounds were identical (15 min, pH 4, 50% v/v ethanol), except the reaction temperature was 37 °C for (±)-H_3RESCA-PEP04314 and 100 °C for H_2NOTA-PEP04314. For this particular affibody (PEP04314), no thermal degradation products were observed, even after 15 minutes incubation at 100 °C. The crude reaction mixtures were purified using preparative RP-HPLC to give (±)-[^{18}F]AlF(RESCA)-PEP04314 or [^{18}F]AlF(NOTA)-PEP04314 in high radiochemical purity (> 98% for both compounds) and with apparent molar radioactivity of respectively 23.2 ± 3.4 GBq/µmol and 21.6 ± 5.4 GBq/µmol at the end of purification. Total synthesis time, starting from [^{18}F]F$^-$, was less than 30 minutes for both compounds. PET/CT studies in healthy male non-human primates were performed to evaluate the distribution profile and *in vivo* stability of both (±)-[^{18}F]AlF(RESCA)-PEP04314 (n=3) and [^{18}F]AlF(NOTA)-PEP04314 (n=6).

Preclinical studies have shown that the nature of the chelator might have a significant effect on the biodistribution of affibody molecules. However this effect is difficult to predict [54]. The attachment of the macrocyclic chelator, NOTA, to affibody molecules involves one of the carboxylic groups of the chelator. As a result, only two carboxyl groups remain available for chelation of [^{18}F]{AlF}$^{2+}$, forming a neutral complex. In contrast, the RESCA ligand conjugated to affibody molecules has three carboxylic groups available for chelation of [^{18}F]{AlF}$^{2+}$, resulting in a complex with a negative net charge. This net charge might shift elimination more to renal clearance and affect kidney retention. On the other hand, the more lipophilic nature of RESCA derivative (due to the presence of a *trans*-cyclohexyl building block and an additional phenyl ring) in comparison with NOTA could shift the elimination of the radiolabeled affibody to hepatic clearance.

PET/CT images of (±)-[^{18}F]AlF(RESCA)-PEP04314 and [^{18}F]AlF(NOTA)-PEP04314 in a healthy rhesus monkey, with the corresponding time-activity curves and chemical structures, are shown in **Figure 6.** Tissue uptake values ($SUV_{120\text{-}180\ min}$) of both compounds are shown in **Table S3**. Similar distribution profiles were observed for both tracers with slightly slower blood clearance for (±)-[^{18}F]AlF(RESCA)-PEP04314. Radiotracer levels in venous samples were fit to a bi-exponential clearance curve, and alpha and beta clearance half-lives in blood were calculated to be respectively 0.08 ± 0.05 h and 1.09 ± 0.23 h for [^{18}F]AlF(NOTA)-PEP04314 and 0.04 ± 0.01 h and 2.70 ± 0.43 h for (±)-[^{18}F]AlF(RESCA)-PEP04314. The sum of percentage injected dose (%ID) in kidneys and urinary bladder (average 120-180 min p.i) was 28.8 ± 2.4 %ID for (±)-[^{18}F]AlF(RESCA)-PEP04314 and 29.9 ± 3.7 %ID for [^{18}F]AlF(NOTA)-PEP04314. This indicates that the difference in net charge and lipophilicity of the chelator seem to compensate each other, resulting in a similar renal clearance pattern for both compounds.

Higher liver uptake was observed for (±)-[^{18}F]AlF(RESCA)-PEP04314 at early time points, probably due to the slower blood clearance (**Figure 6**). However, significantly lower retention in kidney cortex was observed for (±)-[^{18}F]AlF(RESCA)-PEP04314 (standardized uptake value 120-180 min after tracer administration ($SUV_{120\text{-}180\ min}$) 32.5 ± 8.2) than [^{18}F]AlF(NOTA)-PEP04314 ($SUV_{120\text{-}180\ min}$: 56.8 ± 11.0), and higher accumulation of (±)-[^{18}F]AlF(RESCA)-PEP04314 in the bladder was also observed in the PET/CT images. The $\%ID_{120\text{-}180\ min}$ in bladder was 10.6 ± 0.8 %ID for

(±)-[^{18}F]AlF(RESCA)-PEP04314 and only 3.8 ± 1.0 %ID for [^{18}F]AlF(NOTA)-PEP04314. The use of residualizing radiometals, including [^{18}F]AlF(NOTA) complexes [25], results in extended retention of radioactivity in kidneys because these stable radiocomplexes are not able to diffuse out of the proximal tubuli cells. This may cause high radiation burden to the kidneys, hinder diagnostic accuracy, and limit therapeutic applications. Compared to [^{18}F]AlF(NOTA)-PEP04314, (±)-[^{18}F]AlF(RESCA)-PEP04314 shows less activity accumulating in the kidneys due to faster clearance to the bladder. Nonetheless, retention in kidneys is still high compared to non-residualizing ^{18}F-labeling strategies for affibody molecules such as the prosthetic group approach using [^{18}F]FBEM [62]. The residualizing effect is not only important regarding kidney retention, but might also occur in target cells of interest (e.g. cancer cells) if there is a high rate of internalization. In tumor cells the residualizing effect is beneficial, as tumor uptake will be higher and last longer.

Importantly, only minor bone uptake was observed for both tracers, with slightly higher values for (±)-[^{18}F]AlF(RESCA)-PEP04314 ($SUV_{120\text{-}180\ min}$ 2.3 ± 0.7) than [^{18}F]AlF(NOTA)-PEP04314 ($SUV_{120\text{-}180\ min}$ 1.0 ± 0.3), indicating high *in vivo* stability of both tracers in rhesus monkeys. The increasing bone uptake observed for (±)-[^{18}F]AlF(RESCA)-PEP04314 over time indicates that the Al^{18}F-complex formed with the macrocyclic chelator NOTA shows somewhat higher *in vivo* stability than the Al^{18}F-complex formed with the acyclic chelator RESCA, confirming the trade-off between reactivity of the chelators towards [^{18}F]{AlF}$^{2+}$ and the *in vivo* stability of the resulting complexes.

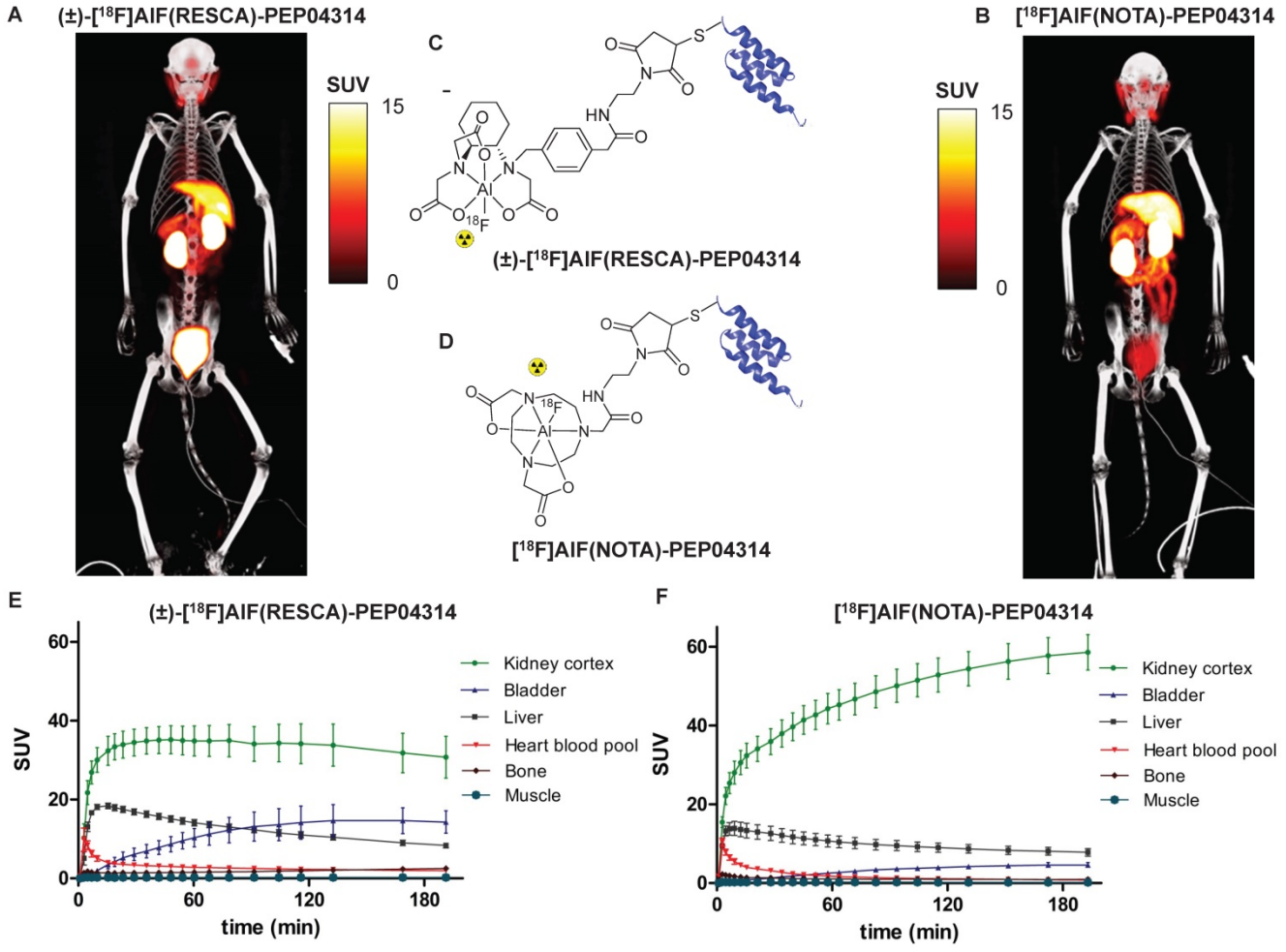

Figure 6. PET/CT imaging of rhesus monkey after intravenous injection of (A) (±)-[^{18}F]AlF(RESCA)-PEP04314 and comparison with (B) [^{18}F]AlF(NOTA)-PEP04314. Summed PET/CT images (120-180 min p.i., time weighted average) performed on healthy rhesus monkey, same animal for both compounds (rhesus monkey A). Structures of (C) (±)-[^{18}F]AlF(RESCA)-PEP04314 and (D) [^{18}F]AlF(NOTA)-PEP04314. Time activity curves (TAC) of different organs after intravenous injection of (E) (±)-[^{18}F]AlF(RESCA)-PEP04314 (n=3) and (F) [^{18}F]AlF(NOTA)-PEP04314 (n=6), data are presented as average standardized uptake values (SUV; tissue activity (MBq/cm^3)/[injected dose (MBq)/body weight (g)]) ± SEM.

Conclusions

Fluorine-18 is currently the radionuclide of choice for PET because of its favorable nuclear decay characteristics and high production capacity. In this study, we show that the Al^{18}F-method using the recently developed chelator RESCA provides an efficient one-step approach to radiolabel heat-sensitive biomolecules at low temperature (< 37°C). We successfully labeled human serum albumin with excellent radiochemical yields in less than 30 minutes and confirmed *in vivo* stability of the Al^{18}F-labeled protein in rats. Moreover, we efficiently labeled nanobodies targeting the Kupffer cell marker CRIg and performed µPET studies in healthy and CRIg deficient mice to demonstrate that the proposed radiolabeling method does not affect the functional integrity of the protein. Finally, an affibody targeting HER2 (PEP04314) was labeled site-specifically, and the distribution profile of (±)-[^{18}F]AlF(RESCA)-PEP04314 in a rhesus monkey was compared with that of [^{18}F]AlF(NOTA)-PEP04314 using whole-body PET/CT. The total synthesis time (starting from [^{18}F]F$^-$) for all compounds was less than 35 minutes, which is considerably shorter than for other radiofluorination methods. Additionally, *in vivo* PET imaging in rats, mice, and non-human primates showed excellent imaging properties for all tracers. This new optimized radiolabeling method can be considered a breakthrough in fluorine-18 radiochemistry. It is easy to implement and can be generically applied for the development of numerous new fluorine-18 labeled heat-sensitive biomolecules.

Abbreviations

{Al^{18}F}$^{2+}$: aluminum mono[^{18}F]fluoride; RESCA: Restrained Complexing Agent; PET: Positron emission tomography; [^{18}F]FDG: 2-[^{18}F]fluoro-2-deoxy-D-glucose; [^{18}F]SFB: *N*-succinimidyl 4-[^{18}F]fluorobenzoate; [^{18}F]F-Py-TFP: 6-[^{18}F]fluoro-nicotinic acid 2,3,5,6-tetrafluorophenyl ester; [^{18}F]FBEM: *N*-[2-(4-[^{18}F]fluorobenzamido)ethyl]maleimide; NODA: 1,4,7-triazacyclononane-1,4-diacetate; NOTA: 1,4,7-triazacyclononane-1,4,7-triacetate; HSA: Human serum albumin; RCY: radiochemical yield; RCP: radiochemical purity; Nb: nanobody; CRIg: complement receptor of the Ig superfamily; RA: rheumatoid arthritis; SUV: standardized uptake value.

Acknowledgements

The authors thank Julie Cornelis, Ivan Sannen, Pieter Haspeslagh and Jana Hemelaers from the Laboratory for Radiopharmaceutical Research, and Ann Van Santvoort, Tine Buelens, Michel Koole, Andrey Postnov from the Department of Nuclear Medicine. This research received support from IWT Flanders (SBO 130065 MIRIAD) and FWO (G0D8817N).

Supplementary Material

Supplementary figures and tables.
http://www.thno.org/v07p2924s1.pdf

Competing Interests

The authors have declared that no competing interest exists.

References

1. Weissleder R. Scaling down imaging: molecular mapping of cancer in mice. Nat Rev Cancer. 2002; 2: 1–8.
2. Serdons K, Verbruggen A, Bormans GM. Developing new molecular imaging probes for PET. Methods. 2009; 48: 104–111.
3. Le Bars D. Fluorine-18 and medical imaging: Radiopharmaceuticals for positron emission tomography. J Fluor Chem. 2006; 127: 1488–1493.
4. Naumova AV, Modo M, Moore A, et al. Clinical imaging in regenerative medicine. Nat Biotechnol. 2014; 32: 804–818.
5. Huyvetter MD, Xavier C, Caveliers V, et al. Radiolabeled nanobodies as theranostic tools in targeted radionuclide therapy of cancer. Expert Opin Drug Deliv. 2014; 11: 1939–1954.
6. Boellaard, R, Delgado-Bolton R, Oyen W, et al. FDG PET/CT: EANM procedure guidelines for tumour imaging: version 2. Eur J Nucl Med Mol Imaging. 2015; 42: 328–354.
7. Wadsak W, Mitterhauser M. Basics and principles of radiopharmaceuticals for PET / CT. Eur J Radiol. 2010; 73: 461–469.
8. Smith GE, Sladen HL, Biagini SCG, et al. Inorganic approaches for radiolabelling biomolecules with fluorine-18 for imaging with positron emission tomography. Dalton Trans. 2011; 40: 6196–6205.
9. Vaneycken I, D'huyvetter M, Hernot S, et al. Immuno-imaging using nanobodies. Curr Opin Biotechnol. 2011; 22: 877–881.
10. De Meyer T, Muyldermans S, Depicker A. Nanobody-based products as research and diagnostic tools. Trends Biotechnol. 2014; 32: 263–270.
11. Wu AM. Engineered antibodies for molecular imaging of cancer. Methods 2014; 65: 139–147
12. Pandit-Taskar N, O'Donoghue JA, Ruan S, et al. First-in-Human Imaging with ^{89}Zr-Df-IAB2M Anti-PSMA Minibody in Patients with Metastatic Prostate Cancer: Pharmacokinetics, Biodistribution, Dosimetry, and Lesion Uptake. J Nucl Med. 2016; 57: 1858-1864.
13. Chakravarty R, Goel S, Valdovinos HF, et al. Matching the Decay Half-Life with the Biological Half-Life: ImmunoPET Imaging with ^{44}Sc-Labeled Cetuximab Fab Fragment. Bioconjug Chem. 2014; 25: 2197−2204.
14. Sharma SK, Wuest M, Way JD, et al. Synthesis and pre-clinical evaluation of an ^{18}F-labeled single-chain antibody fragment for PET imaging of epithelial ovarian cancer. Am J Nucl Med Mol Imaging. 2016; 6: 185–198.
15. Goldstein R, Sosabowski J, Livanos M, et al. Development of the designed ankyrin repeat protein (DARPin) G3 for HER2 molecular imaging. Eur J Nucl Med Mol Imaging. 2015; 42: 288–301.
16. Keyaerts M, Xavier C, Heemskerk J, et al. Assessment of HER2 Expression in Breast Carcinoma. J Nucl Med. 2016; 57: 27–33.
17. Sandström M, Lindskog K, Velikyan I, et al. Biodistribution and Radiation Dosimetry of the Anti-HER2 Affibody Molecule ^{68}Ga-ABY-025 in Breast Cancer Patients. J Nucl Med. 2016; 57: 867–871.
18. Garousi J, Lindbo S, Honarvar H, et al. Influence of the N-terminal composition on targeting properties of radiometal-labeled anti- HER2 scaffold protein ADAPT6. Bioconjug Chem. 2016; 27: 2678–2688.
19. Richter S, Wuest M, Bergman CN, et al. Rerouting the metabolic pathway of $^{(18)}$F-labeled peptides: the influence of prosthetic groups. Bioconjug Chem. 2015; 26: 201–212.
20. Thonon D, Goblet D, Goukens E, et al. Fully Automated Preparation and Conjugation of N-Succinimidyl 4-[^{18}F]Fluorobenzoate ([^{18}F]SFB) with RGD Peptide Using a GEFASTlab™ Synthesizer. Mol Imaging and Biol. 2011; 13: 1088–1095.
21. Olberg DE, Arukwe JM, Grace D, et al. One step radiosynthesis of 6-[$^{(18)}$F]fluoronicotinic acid 2,3,5,6-tetrafluorophenyl ester ([$^{(18)}$F]F-Py-TFP): a new prosthetic group for efficient labeling of biomolecules with fluorine-18. J Med Chem. 2010; 53: 1732–1740.
22. Kiesewetter DO, Jacobson O , Lang L, et al. Automated radiochemical synthesis of [^{18}F]FBEM: A thiol reactive synthon for radiofluorination of peptides and proteins. Appl Radiat Isot. 2011, 69: 410–414
23. Bernard-Gauthier V, Bailey JJ, Liu Z, et al. From Unorthodox to Established: The Current Status of ^{18}F-Trifluoroborate- and ^{18}F-SiFA-Based

Radiopharmaceuticals in PET Nuclear Imaging. Bioconjug Chem. 2015; 27: 267–279.
24. McBride WJ, D'Souza CA, Sharkey RM, et al. The radiolabeling of proteins by the [^{18}F]AlF method. Appl Radiat Isot. 2012; 70: 200–204.
25. McBride WJ, Sharkey RM, Goldenberg DM. Radiofluorination using aluminum-fluoride (Al^{18}F). Eur J Nucl Med Mol Imaging Research. 2013; 3: 36–47.
26. Laverman P, McBride WJ, Sharkey RM, et al. Al$^{(18)}$F labeling of peptides and proteins. J Labelled Comp Radiopharm. 2014; 57: 219–223.
27. Wang W, Liu Z, Li Z. One-Step ^{18}F Labeling of Non-Peptidic Bivalent Integrin α. Bioconjug Chem. 2015; 26: 24–28.
28. Kiesewetter DO, Guo N, Guo J, et al. Evaluation of an [$^{(18)}$F]AlF-NOTA Analog of Exendin-4 for Imaging of GLP-1 Receptor in Insulinoma. Theranostics. 2012; 2: 999–1009.
29. Da Pieve C, Allott L, Martins CD, et al. Efficient [^{18}F]AlF Radiolabeling of ZHER3:8698 Affibody Molecule for Imaging of HER3 Positive Tumors. Bioconjug Chem. 2016; 27: 1839–1849.
30. Wan W, Guo N, Pan D, et al. First Experience of ^{18}F-Alfatide in Lung Cancer Patients Using a New Lyophilized Kit for Rapid Radiofluorination. J Nucl Med. 2013; 54: 691–698.
31. Cleeren F, Lecina J, Billaud EMF, et al. New chelators for low temperature Al^{18}F-labeling of biomolecules. Bioconjug Chem. 2016; 27: 790–798.
32. Bormans GM, Cleeren F, Lecina J, et al. Methods for low temperature fluorine-18 radiolabelling of biomolecules (WO/2016/065435).
33. Zheng F, Put S, Bouwens L, et al. Nanobodies for Early and Preclinical Diagnosis in a Mouse Model of Rheumatoid Arthritis. J Nucl Med. 2014; 55: 824–830.
34. Wetzel R, Becker M, Behlke J, et al. Temperature behaviour of human serum albumin. Eur J Biochem. 1980; 104: 469–478.
35. Bernardi M, Ricci CS, Zaccherini G. Role of human albumin in the management of complications of liver cirrhosis. J Clin Exp Hepatol. 2014; 4: 302–311.
36. Basuli F, Li C, Xu B, et al. Synthesis of fluorine-18 radio-labeled serum albumins for PET blood pool imaging. Nucl Med Biol. 2015; 42: 219–225.
37. Ramenda T, Kniess T, Bergmann R, et al. Radiolabelling of proteins with fluorine-18 via click chemistry. Chem Commun. 2009; 48: 7521–7523.
38. Jadvar H, Desai B, Conti PS. Sodium ^{18}F-fluoride PET/CT of bone, joint, and other disorders. Semin Nucl Med. 2015; 45: 58–65.
39. Chatalic KLS, Franssen GM, Van Weerden WM, et al. Preclinical comparison of Al^{18}F- and ^{68}Ga-labeled gastrin-releasing peptide receptor antagonists for PET imaging of prostate cancer. J Nucl Med. 2014; 55: 2050–2056.
40. Lafage-Proust MH, Roche B, Langer M, et al. Assessment of bone vascularization and its role in bone remodeling. BoneKEy Rep. 2015; 4: 1-8.
41. De Vos J, Devoogdt N, Lahoutte T, et al. Camelid single-domain antibody-fragment engineering for (pre)clinical in vivo molecular imaging applications: adjusting the bullet to its target. Expert Opin Biol Ther. 2013; 13: 1149–1160.
42. D'Huyvetter M, Vincke C, Xavier C, et al. Targeted radionuclide therapy with A ^{177}Lu-labeled anti-HER2 nanobody. Theranostics. 2014; 4: 708–720.
43. Xavier C, Vaneycken I, D'huyvetter M, et al. Synthesis, Preclinical Validation, Dosimetry, and Toxicity of ^{68}Ga-NOTA-Anti-HER2 Nanobodies for iPET Imaging of HER2 Receptor Expression in Cancer. J Nucl Med. 2013; 54: 776–784.
44. Xavier C, Blykers A, Vaneycken I, et al. ^{18}F-nanobody for PET imaging of HER2 overexpressing tumors. Nucl Med Biol. 2016; 43: 247–252.
45. Blykers A, Schoonooghe S, Xavier C, et al. PET imaging of MMR-expressing macrophages in tumor stroma using ^{18}F-radiolabeled camelid single-domain antibody fragments. J Nucl Med. 2015; 56: 1265-1271.
46. Bala G, Blykers A, Xavier C, et al. Targeting of vascular cell adhesion molecule-1 by ^{18}F-labelled nanobodies for PET/CT imaging of inflamed atherosclerotic plaques. Eur Heart J Cardiovasc Imaging. 2016; 17: 1001–1008.
47. Wen Y, Ouyang Z, Schoonooghe S, et al. Structural evaluation of a nanobody targeting complement receptor Vsig4 and its cross reactivity. Immunobiology; in press.
48. Helmy KY, Katschke KJ, Gorgani NN, et al. CRIg: A macrophage complement receptor required for phagocytosis of circulating pathogens. Cell. 2006; 124: 915–927.
49. Zheng F, Sparkes A, De Baetselier P, et al. Molecular Imaging with Kupffer Cell-Targeting Nanobodies for Diagnosis and Prognosis in Mouse Models of Liver Pathogenesis. Mol Imaging Biol. 2017; 19: 49-58.
50. Gainkam LOT, Caveliers V, Devoogdt N, et al. Localization , mechanism and reduction of renal retention of technetium-99m labeled epidermal growth factor receptor-specific nanobody in mice. Contrast Media Mol Imaging. 2011; 6: 85–92.
51. Bondos SE, Bicknell A. Detection and prevention of protein aggregation before, during, and after purification. Analytical biochemistry. 2003; 316: 223-231.
52. Nygren PA. Alternative binding proteins: Affibody binding proteins developed from a small three-helix bundle scaffold. FEBS J. 2008; 275: 2668–2676.
53. Strand J, Nordeman P, Honarvar H, et al. Site-Specific Radioiodination of HER2-Targeting Affibody Molecules using 4-Iodophenethylmaleimide Decreases Renal Uptake of Radioactivity. ChemistryOpen. 2015; 4: 174–182.
54. Westerlund K, Honarvar H, Norrström E, et al. Increasing the Net Negative Charge by Replacement of DOTA Chelator with DOTAGA Improves the Biodistribution of Radiolabeled Second-Generation Synthetic Affibody Molecules. Mol Pharm. 2016; 13: 1668-1678.
55. Krämer-Marek G, Shenoy N, Seidel J, et al. ^{68}Ga-DOTA-Affibody Molecule for In Vivo Assessment of HER2/ neu Expression with PET. Eur J Nucl Med Mol Imaging. 2011; 38: 1967–1976.
56. Kiesewetter DO, Krämer-Marek G, Ma Y, et al. Radiolabeling of HER2 specific Affibody molecule with F-18. J Fluor Chem. 2008; 129: 799–805.
57. Cheng Z, De Jesus OP, Kramer DJ, et al. ^{64}Cu-Labeled Affibody Molecules for Imaging of HER2 Expressing Tumors. Mol Imaging Biol. 2010; 12: 316–324.
58. Ahlgren S, Wallberg H, Tran TA, et al. Targeting of HER2-Expressing Tumors with a C-Terminally Engineered Cysteine. J Nucl Med. 2009; 50: 781–789.
59. Perols A, Honarvar H, Strand J, et al. Influence of DOTA Chelator Position on Biodistribution and Targeting Properties of ^{111}In-Labeled Synthetic Anti-HER2 Affibody Molecules. Bioconjug Chem. 2012; 23: 1661–1670.
60. Price EW, Orvig C. Matching chelators to radiometals for radiopharmaceuticals. Chem Soc Rev. 2014; 43: 260–290.
61. Heskamp S, Laverman P, Rosik D, et al. Imaging of Human Epidermal Growth Factor Receptor Type 2 Expression with ^{18}F-Labeled Affibody Molecule $Z_{HER2:2395}$ in a Mouse Model for Ovarian Cancer. J Nucl Med. 2012; 53: 146–153.
62. Kramer-Marek G, Kiesewetter DO, Martiniova L, et al. [^{18}F]FBEM-$Z_{HER2:342}$–Affibody molecule—a new molecular tracer for in vivo monitoring of HER2 expression by positron emission tomography. Eur J Nucl Med Mol Imaging. 2008; 35: 1008–1018.